J Neurophysiol 99: 1253–1266, 2008.
First published January 23, 2008; doi:10.1152/jn.01096.2007.

Neuronal Activity in the Cingulate Motor Areas During Adaptation to a New Dynamic Environment

Andrew G. Richardson,[1,*] Glenda Lassi-Tucci,[2,*] Camillo Padoa-Schioppa,[3] and Emilio Bizzi[2]

[1]*Division of Health Sciences and Technology, Massachusetts Institute of Technology and Harvard Medical School;* [2]*Department of Brain and Cognitive Sciences and McGovern Institute for Brain Research, Massachusetts Institute of Technology, Cambridge; and* [3]*Department of Neurobiology, Harvard Medical School, Boston, Massachusetts*

Submitted 3 October 2007; accepted in final form 18 January 2008

Richardson AG, Lassi-Tucci G, Padoa-Schioppa C, Bizzi E. Neuronal activity in the cingulate motor areas during adaptation to a new dynamic environment. *J Neurophysiol* 99: 1253–1266, 2008. First published January 23, 2008; doi:10.1152/jn.01096.2007. Neurons in the cingulate motor areas (CMA) have been shown to be involved in many aspects of sensorimotor behavior, although their role in motor learning has received less attention. Here, we recorded single-cell activity in the CMA of monkeys while they adapted reaching movements to different dynamic environments. Specifically, we analyzed CMA activity during normal reaching to visual targets and during reaching in the presence of an applied velocity-dependent force field. We found that the cingulate neuronal activity was modulated during each phase of the task and in response to the applied forces. The neurons' involvement in the visuomotor transformation was influenced by their rostrocaudal location in the cingulate sulcus. Rostral CMA (CMAr) neurons were modulated by the visual instruction to a greater extent than caudal CMA (CMAc) neurons. In contrast, CMAc neurons had a greater amount of phasic and directionally tuned activity during movement than CMAr cells. Furthermore, compared with CMAr cells, the movement-related activity of CMAc cells was more frequently modulated by the applied force fields. The magnitude of the force-field–related neuronal response scaled with the amount of perturbation in each reaching direction. However, contrary to previous results from other cortical motor areas, force-field adaptation was not correlated with a shift in directional tuning of the CMA population. Based on these results, we suggest that although the CMA is clearly sensitive to applied forces, it is less involved in generating anticipatory responses to predictable forces than other cortical motor areas.

INTRODUCTION

Anatomical studies have identified multiple distinct premotor areas in the primate frontal lobe, each of which projects directly to primary motor cortex and the spinal cord (Dum and Strick 2002). Understanding the differential contribution of these areas to motor control and motor learning is a matter of ongoing research. This is particularly true of the cingulate motor areas (CMA), located within the cingulate sulcus on the medial wall of the cerebral hemisphere, whose neuronal activity has only recently been studied (Akkal et al. 2002; Backus et al. 2001; Cadoret and Smith 1995, 1997; Crutcher et al. 2004; Hoshi et al. 2005; Russo et al. 2002; Shidara and Richmond 2002; Shima and Tanji 1998; Shima et al. 1991). These studies have shown that single-cell activity in the CMA is correlated with the preparation, execution, and reward of motor behaviors. Similar movement-related CMA activity has been demonstrated by functional imaging in humans (Fink et al. 1997; Picard and Strick 1996).

Human imaging work suggests that the CMA are also involved in several types of motor learning. Learning-related increases in CMA activity have been observed when learning a sequence of movements (Doyon et al. 1996; Grafton et al. 1998), learning a conditional visuomotor association (Deiber et al. 1997), and adapting to a visuomotor transformation (Della-Maggiore and McIntosh 2005). However, similar investigations into motor learning have not been conducted at the single-cell level in the CMA. Therefore we studied CMA neuronal activity during a motor-learning task. In particular, monkeys were trained to make reaching movements that, at times, were perturbed by a novel pattern of velocity-dependent forces, or a curl force field (Shadmehr and Mussa-Ivaldi 1994). Monkeys adapted their movements to the force-field environment and, when the force field was suddenly removed, showed prominent adaptation aftereffects.

In a series of previous studies, we found that the activity of many neurons throughout the motor areas of the frontal lobe was correlated with force-field adaptation (Gandolfo et al. 2000; Li et al. 2001; Padoa-Schioppa et al. 2002, 2004; Xiao et al. 2006). Specifically, we observed that the relationship between cell spike rate and movement direction gradually changed when learning the force-field environment to provide appropriate compensatory muscle activity. The goal of the present study was to complete this line of investigation of cortical motor areas by recording neuronal activity in the CMA during force-field adaptation. It is known that CMA activity is modulated by force production in humans (Dettmers et al. 1995; Ehrsson et al. 2007; Kuhtz-Buschbeck et al. 2001) and monkeys (Cadoret and Smith 1995, 1997). Therefore we predicted CMA neuronal activity would be modulated by the applied force fields and exhibit adaptation-related changes in directional tuning.

In the present study, intracortical microstimulation revealed distinct rostral (CMAr) and caudal (CMAc) limb representations. Cells in each representation were engaged in the preparatory and movement phases of the visuomotor reaching task. Furthermore, the applied forces caused the movement-related activity of some CMA neurons, predominantly located in the CMAc, to increase in a reflex-like manner. However, a shift in directional tuning of neuronal activity—the hallmark of force-

* These authors contributed equally to this work.
Address for reprint requests and other correspondence: E. Bizzi, Massachusetts Institute of Technology, MIT 46-6189, 43 Vassar Street, Cambridge, MA 02139 (E-mail: ebizzi@mit.edu).

The costs of publication of this article were defrayed in part by the payment of page charges. The article must therefore be hereby marked "*advertisement*" in accordance with 18 U.S.C. Section 1734 solely to indicate this fact.

field adaptation seen in other cortical motor areas—was not as prominent in the CMA.

METHODS

Two male rhesus macaques (*Macaca mulatta*), C and K, were involved in this experiment. The behavioral task and electrophysiological techniques were very similar to those of our previous studies (Gandolfo et al. 2000; Li et al. 2001; Padoa-Schioppa et al. 2002, 2004; Xiao et al. 2006). All experimental procedures adhered to the National Institutes of Health *Guide for the Care and Use of Laboratory Animals* and were approved by the MIT Committee for Animal Care.

Behavioral task

The monkeys sat in a chair and held on to a handle at the end of a two-link, planar robotic manipulandum with their right hand (Fig. 1*A*). On each trial, they moved the handle in the horizontal plane between two targets located 8 cm apart. The targets (1.6-cm white squares) and current position of the handle (a 0.3-cm white square) read from potentiometers on the robotic arm were indicated on a monitor with a black background placed about 75 cm in front of the monkey.

Each trial began with a 1-s hold time at the center target, followed by the presentation of a pseudorandomly chosen peripheral target (i.e., the cue). The peripheral target was in one of eight locations, spaced uniformly 45° apart in a circle around the center target. The center target remained on for a variable 0.5 to 1.5 s after the cue to indicate the instructed delay time. On disappearance of the center target (i.e., the go signal), the monkey made a reaching movement to place the cursor in the peripheral target, where it had to remain for 1 s to receive a juice reward. Thus the reaching task consisted of five behavioral intervals (center hold; delay time; reaction time; movement time; target hold) divided by four events (peripheral target on, *cue*; center target off, *go*; movement onset, *mo*; movement end, *me*) (Fig. 1*B*).

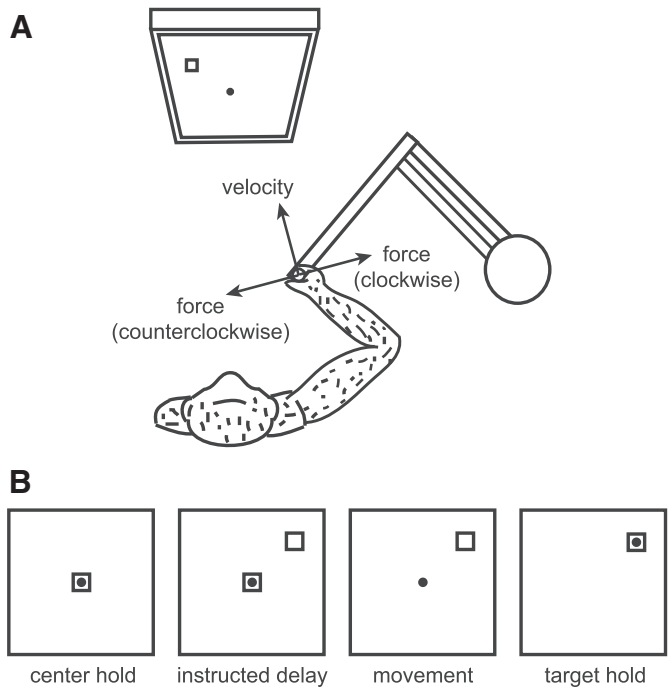

FIG. 1. Behavioral task. *A*: schematic of the approximate relative orientation of the monkey, robotic arm, and monitor. Forces applied to the arm were proportional and perpendicular (either clockwise or counterclockwise) to the hand velocity vector. *B*: schematic of the cursor (circle) and targets (squares) on the monitor during the 4 phases of each trial.

Movement duration had to be <3 s and movements had to remain at all times within a region ±60° about a line connecting the center and peripheral targets. Any error resulted in abortion of the trial without reward. The hand trajectory (position and velocity) on each trial was recorded at 100 Hz.

In control sessions, the monkeys performed ≥480 correct trials with no external forces (i.e., a null force field). In learning sessions, the monkeys performed 160 correct trials with no external forces (baseline epoch), followed immediately by another 160 correct trials during which the robotic manipulandum applied forces on the hand that were proportional and perpendicular to its velocity vector (force-field epoch), and finally another 160 correct trials with no external forces (washout epoch). The magnitude of the velocity-dependent curl force field was 6 Ns/m. In the learning sessions, the force field could be either clockwise or counterclockwise. Thus overall, the monkeys performed reaching movements in three types of force fields: null field, clockwise curl field, or counterclockwise curl field.

Surgery

All surgeries were performed using sterile techniques with the monkey under general anesthesia. After sufficient training on the task, a stainless steel head-restraining device was fixed to the skull near lambda. The monkey was then retrained to perform the task under head-fixed conditions. Then a 28-mm circular craniotomy was performed, leaving the dura mater intact, and a stainless steel recording well was fixed to the skull around this site. The center of the craniotomy was 23 mm (monkey K) or 22 mm (monkey C) rostral to the interaural line and centered on the midline. Systemic antibiotics and analgesics were given following the surgeries and the monkeys were allowed several days of rest to recover from each procedure. The exposed dura mater was treated with topical antibiotics and antiinflammatories daily. Periodically (once every ~2–3 wk), scarring that would accumulate over the dura mater was mechanically removed.

Electrophysiology

Intracortical microstimulation (ICMS) was used to map the somatic representations of the medial cortical motor areas of the left hemisphere. ICMS consisted of 50-ms trains of biphasic pulses at 330 Hz, with 0.2-ms pulse duration and 10- to 120-μA pulse amplitude. Stimulus-evoked muscle twitches were observed and mapped to the cortical location of the stimulus. After the ICMS study, extracellular recordings were made during each session that the monkeys performed the task, mostly from cortical locations at which the arm was represented. For the stimulations and recordings, we used epoxylite-insulated tungsten microelectrodes, with 1- to 3-MΩ impedance and 250-μm-diameter shaft tapered down to a 3-μm-diameter tip (FHC). The electrodes were lowered transdurally at the beginning of each session using a custom-made manual microdrive with a depth resolution of about 30 μm. Due to dimpling of the cortex on penetration and limitations in depth resolution, the laminar location of the recorded cortical cells was generally not known. Up to eight electrodes were used in each recording session. The analog electrical signals from the electrodes were passed first to a preamplifying headstage (AI 401, Axon Instruments) located about 5 cm from the electrodes, then to an amplifier (Cyberamp 380, Axon Instruments) where they were filtered (300-Hz to 10-kHz passband) to obtain multiunit activity, and finally to an A/D board where they were digitized (12-bit resolution at 20 kHz/channel). The multiunit activity was not recorded continuously, but rather action potentials (i.e., spikes) were detected on-line by a manually determined threshold crossing and only the spike times, along with behavioral task event times, were recorded to file with 0.1-ms resolution. Spike waveforms (i.e., 1.75 ms of the continuous signal around the spike time) were also saved for subsequent off-line spike sorting.

Anatomy and histology

At the end of the recording sessions, the boundaries of the recording sites were marked with electrolytic lesions (cathodal current, 20 μA, 2 min). Then the monkeys were given an overdose of pentobarbital sodium and perfused transcardially with heparinized saline followed by buffered formalin. India ink was used to mark the surface of the cortex at selected coordinates near the recording sites. The brains were then removed from the skull and photographed to record anatomical landmarks relative to the recording sites. The brains were sectioned (coronal plane, 10-μm sections) and stained (luxol fast blue and cresyl echt violet) for histological analysis.

Behavioral analysis

Performance was quantified on each successful trial by the signed deviation area between the hand path and the line connecting the center and peripheral targets (Rokni et al. 2007). To assess robustness of our results we also computed two other performance metrics: the peak perpendicular displacement of the hand path from a straight line (Shadmehr and Moussavi 2000) and the perpendicular displacement of the hand path 250 ms after movement onset from a straight line (Thoroughman and Shadmehr 2000). All three performance metrics yielded very similar results; for brevity we report the results using the deviation area measure only. We also looked at the trial success rate, but it did not generally capture the performance as well as the trajectory-based measures. All aborted trials were excluded from the analysis.

Force-field–related changes in performance were tested with five planned comparisons (*t*-test) for each session: *1*) an adaptation test (trials 161–200, *ii* in Fig. 2, vs. 281–320, *iii*), *2*) an aftereffect test (trials 121–160, *i*, vs. 321–360, *iv*), *3*) a deadaptation test (trials 321–360, *iv*, vs. 441–480, *v*), *4*) a completeness of adaptation test (trials 121–160, *i*, vs. 281–320, *iii*), and *5*) a completeness of deadaptation test (trials 121–160, *i*, vs. 441–480, *v*). A per comparison error rate ($P < 0.05$) was used to judge significance since only the overall percentage of significant tests across sessions was of interest (conservatively assuming $\leq$5% were type I errors).

In addition to the preceding comparisons, which lumped together trials in all eight target directions, we assessed whether performance changes due to the perturbation (early force-field, trials 161–200, *ii*) or due to aftereffects (early washout, trials 321–360, *iv*) were directionally tuned. Changes were defined relative to the mean late baseline (*i*) performance in the corresponding directions. For each monkey, performance changes were compiled across all learning sessions, separating clockwise from counterclockwise. The four data sets (perturbation or aftereffect changes due to clockwise or counterclockwise force fields) were subjected to Rayleigh tests for uniformity across directions with a unimodal alternative and with a bimodal alternative (Fisher 1993), using Moore's modification for weighted directional data (Moore 1980).

Neuronal analysis

Spike sorting was done manually, with the aid of a software package (Autocut 3, DataWave Technologies), by detecting clusters in spike waveform feature space. Clusters of spikes were assumed to come from one neuron if they were *1*) reasonably separated from other clusters and noise spikes in feature space; *2*) had temporally continuous, if not constant, waveform features; and *3*) exhibited at least a 1-ms refractory period. Spike clusters meeting these criteria were classified as single-unit activity (i.e., neuronal activity).

We examined how neuronal activity, and in particular the rate of spiking, was modulated by within-trial events, such as the *cue* or *go* signals (event-related activity) and across-trial changes in the dynamic environment (force-field–related activity). The time windows and trial epochs used to compute spike rate differed for these two analyses. For the event-related analysis, we used the concatenation of three

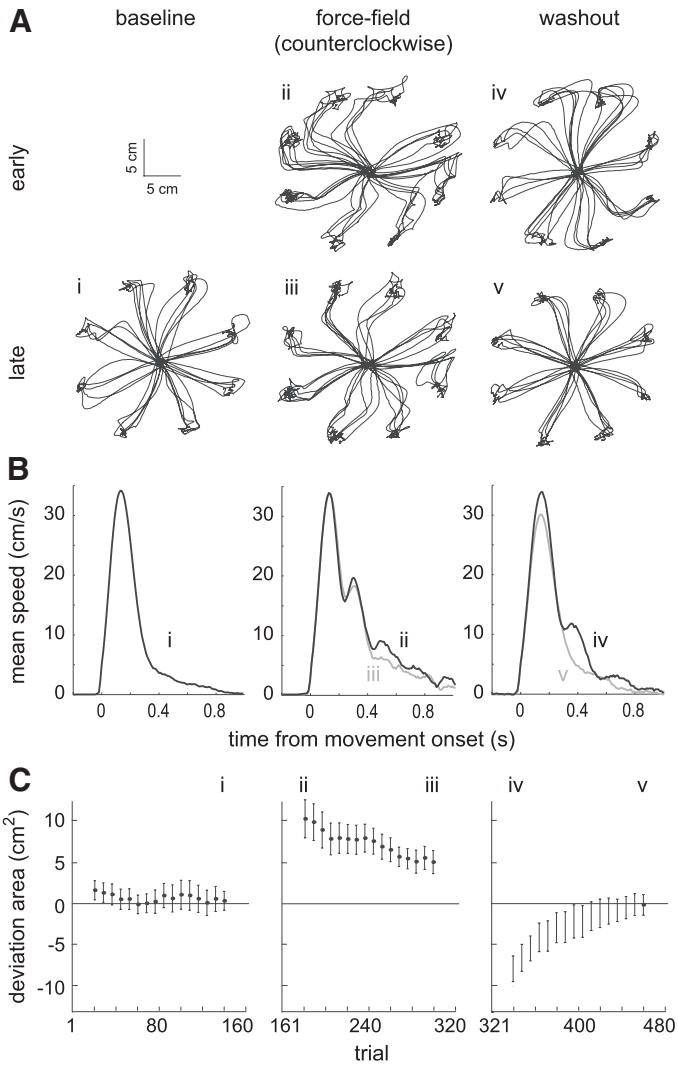

FIG. 2. Example of behavioral performance during one session (monkey C). *A*: hand paths from the center target to each of the 8 peripheral targets during the first 40 trials (early) or last 40 trials (late) of each epoch (baseline, force-field, washout). *B*: average hand speed during each of the 40-trial blocks shown in *A*. *C*: moving average of performance during each epoch [40-trial mean, 95% confidence interval for mean, 8-trial step, no averaging across epoch boundaries], as quantified by the signed deviation area of the hand paths relative to a straight line. Roman numerals indicate the correspondence between the hand paths (*A*), the speed profiles (*B*), and the computed performance (*C*).

perievent time windows spanning the trial (center hold/instructed delay time, *cue* − 1,000 ms to *cue* + 1,000 ms; reaction/movement time, *mo* − 400 ms to *mo* + 400 ms; and target hold time, *me* − 100 ms to *me* + 1,000 ms) and the last 120 trials of the baseline epoch. Instantaneous spike-rate profiles were computed by convolving the spike trains of each trial with a Gaussian kernel (50 ms SD) and averaging over the 120 trials (although see subsequent paragraph on directional selectivity). The result was a 3.9-s profile of baseline activity for each cell. Very similar profiles could be obtained if washout, rather than baseline, trials were used. For the force-field–related analysis, we used a movement time window (*mo* − 100 ms to *mo* + 400 ms) and the last 40 trials of the baseline epoch, all 160 trials of the force-field epoch, and the first 40 trials of the washout epoch. Instantaneous spike-rate profiles were computed by calculating the spike count rate in the movement time window on each trial and convolving the rates with a Gaussian kernel (10 trial SD) within each epoch separately. The smoothed spike rates of the three epochs were

concatenated together to produce a 240-trial profile of movement time activity for each cell. Exploratory analysis revealed very little force-field–related activity in other, non-movement time windows.

After computing the two spike-rate profiles for each cell, we determined whether the profiles were significantly modulated. We defined a statistic, the modulation index, which quantified whether each profile had a relative constant spike rate or had a spike rate that fluctuated over time (event-related profile) or trials (force-field–related profile). For the index, we calculated the median spike rate of the entire profile. Also we calculated the 95% confidence interval on the mean (CIM) for each data point in the profile. The modulation index was defined as the fraction of the profile length (either 3.9 s or 240 trials) in which the lower CIM was greater than the median spike rate (i.e., excitation) and the upper CIM was less than the median spike rate (i.e., inhibition). The modulation index could range from 0 (no modulation) to 1 (continuous modulation). To estimate the distribution of this statistic under the null hypothesis (i.e., no modulation, constant spike rate), we generated surrogate data by simulating stationary Poisson point processes. In particular, we computed the modulation index for 1,000 surrogate "cells," each with 120 Poisson spike trains of 3.9-s duration (for the event-related analysis) or 240 Poisson spike trains of 0.5-s duration (for the force-field–related analysis) that were convolved with the same Gaussian kernel used for the real data. Because the modulation index is sensitive only to modulation duration, not amplitude, the simulated modulation index distribution was largely independent of the chosen constant spike rate of the Poisson spike trains. Nevertheless, we chose the across-cell distribution of spike rates to correspond to that of the real data. The 99th percentile of the generated modulation index distribution was used as the critical value for rejecting the null hypothesis. The critical value of the modulation index (0.16) was the same for both the event-related and force-field–related analyses. The simulations, as well as observation of the real data, indicated that cells with very low but relatively constant spike rates were not always detected by this procedure. Thus we also removed from the analyses cells with average spike rate <0.3 Hz ($n = 27$ in event-related analysis; $n = 0$ in force-field–related analysis).

After determining which spike-rate profiles were significantly modulated, we used cluster analysis to identify subpopulations of cells with similar modulations. For each cell, the spike-rate profiles were z-score transformed (i.e., subtracted the mean and divided by the SD of the 3.9-s baseline activity profile and the 240-trial movement activity profile) to focus only on modulation timing rather than on modulation amplitude. Then the *k*-means clustering algorithm was applied to either all of the within-trial profiles (event-related analysis) or all the across-trial profiles (force-field–related analysis). The algorithm iteratively defined clusters of activity patterns by minimizing the within-cluster sum of distances from the cluster centroids. Distance was defined to be squared Euclidean distance. Other distance measures produced very similar results. To compensate for the potential convergence of the algorithm to local minima, the clustering procedure was repeated 100 times with randomly selected initial centroid locations. The repetition with the least error was chosen. The number of clusters (k) was chosen subjectively, although the major results of the analysis were evident across many values of k. Two-way contingency table tests, Pearson's chi-squared (χ^2), were used to determine whether there was a relationship between the activity pattern clusters and other classifying variables (e.g., cortical area, type of force field in which the cell was recorded).

In both the event-related and force-field–related analyses, we also studied modulations in directional selectivity of spiking. Significance of directional selectivity was based on a one-tailed permutation test on the resultant vector magnitude (*rvm*; i.e., the magnitude of the sum of vectors whose direction is defined by the target direction on a given trial and magnitude is defined by the spike rate). Distribution of the *rvm* under the null hypothesis (i.e., no tuning, uniform or antipodal symmetric distribution of spike rates across target directions) was obtained by shuffling the relationship between trial and direction, computing the *rvm* for this shuffled data, and repeating these two steps 1,000 times. If fewer than ten values from this distribution were greater that the actual *rvm*, the tuning was considered to be significant ($P < 0.01$). When the directional tuning was significant, the preferred direction of the tuning curve (i.e., the resultant vector direction) was computed. In the event-related analysis, the instantaneous tuning significance was computed by applying this procedure every 10 ms, resulting in a 3.9-s-duration binary vector for each cell where zero indicated no tuning and one indicated tuning. The mean instantaneous spike rate, used in both the modulation index computation and the cluster analysis, was then based on the average over trials in all eight directions when the tuning was not significant and over trials in the four directions closest to the preferred direction (i.e., the preferred hemifield) when the tuning was significant. The clustering methods were then applied to both the population of instantaneous preferred-hemifield spike-rate profiles, as described earlier, and the population of instantaneous tuning significance profiles. The latter clustering analysis used Hamming distance (i.e., percentage of differing bits between binary vectors), instead of squared Euclidean distance, for the distance measure. In the force-field–related analysis, directional selectivity could not be defined instantaneously over trials using our methods. Clustering was simply applied to the across-trial spike-rate profiles that, due to the Gaussian smoothing and pseudorandom ordering of target directions, were effectively an average of spike rates across all eight target directions. For an analysis of force-field–related directional modulation, one directional tuning curve per epoch was computed, using the last 120 trials of the epoch (Li et al. 2001), and then the three tuning curves were compared.

Finally, we performed additional analyses to verify the results of the cluster analysis. In particular, for the event-related activity we performed a conventional ANOVA. For each of the last 120 baseline trials, the spike count rate was computed within four, 500-ms perievent windows to quantify cue-related activity (postcue window, *cue* + 50 ms to *cue* + 550 ms), instructed delay-related activity (delay-time window, *cue* + 450 ms to *cue* + 950 ms), movement-related activity (movement-time window, *mo* − 100 ms to *mo* + 400 ms), and target hold–related activity (target hold window, *me* + 500 ms to *me* + 1,000 ms). The activity in each of these four windows was compared with control activity (center-hold window, *cue* − 750 ms to *cue* − 250 ms) using a two-way ANOVA with window and target direction as factors. We reported only the main effects of window and interaction effects of window × direction. Main effects of direction were redundant since control activity was not directionally tuned and thus they were almost entirely due to window × direction interactions.

RESULTS

Psychophysics

Two monkeys (K and C) were trained to make reaching movements from a center target to one of eight peripheral targets while holding onto a robotic manipulandum capable of applying perturbing forces to the arm (Fig. 1*A*). Each session began with 160 trials without forces (baseline epoch). Despite the loose regulation of hand path (see METHODS), the movements during the baseline epoch were quite straight (Fig. 2*A*, *i*) and the average speed profiles were monophasic (Fig. 2*B*, *left*). To quantify the straightness, on each trial we computed the signed area between the hand path and a straight line connecting the center and peripheral targets. The mean deviation area was generally near zero throughout the baseline epoch (Fig. 2*C*, *left*). In the 160 trials following the baseline epoch, forces were applied that were proportional and perpendicular (either counterclockwise or clockwise) to the hand velocity vector

(force-field epoch). This perturbing force field caused the hand paths to become curved (Fig. 2*A*, *ii*) and velocity profiles to have multiple peaks (Fig. 2*B*, *middle*). With experience the paths became straighter, indicating that the monkeys adapted to the forces, although, as in the example in Fig. 2, often the adaptation was not complete (i.e., nonzero deviation area; Fig. 2*C*, *middle*). Finally, the forces were turned off and the monkeys performed a final 160 trials in the null-field environment (washout epoch). Abruptly turning off the forces led to an adaptation aftereffect; the hand paths became curved again but this time in the direction opposite to that seen in the early force-field epoch (Fig. 2, *iv*). With continued practice in the washout epoch, once again the hand paths became straight and velocity profiles monophasic, indicating the monkeys had deadapted back to the original conditions (Fig. 2, *v*).

The adaptation, aftereffect, and deadaptation can be seen clearly in the time course of deviation area changes (Fig. 2*C*, *ii* to *iii*, *i* to *iv*, and *iv* to *v*, respectively). We tested whether these changes were statistically significant in each session (*t*-test, $P < 0.05$). Of the sessions in which the monkeys were exposed to either a clockwise or counterclockwise force field ($n = 16$ sessions, monkey K; $n = 13$ sessions, monkey C), the adaptation effect was significant in 100% of sessions for monkey K and 69% of sessions for monkey C. The aftereffect and deadaptation effect were significant in 100% of sessions for both monkeys. Although it is seemingly contradictory to have adaptation aftereffects and deadaptation without adaptation in some sessions, significant cocontraction of arm muscles at the beginning of the force-field epoch could mask adaptation as we define it (i.e., a change in the straightness of the hand trajectory from early to late force-field epoch trials). Indeed, work in humans suggests that the initial phase of learning novel environments is dominated by an increase in arm stiffness, which eventually subsides once an internal model of the environment is formed (Franklin et al. 2003; Osu et al. 2002, 2003; Thoroughman and Shadmehr 1999). Thus in all sessions the monkeys learned to proactively compensate for the applied forces.

Similarly we tested the completeness of adaptation and deadaptation (Fig. 2*C*, deviation area changes from *i* to *iii* and *i* to *v*, respectively). Adaptation was incomplete in 6 of 16 sessions (38%) in monkey K and 7 of 13 sessions (54%) in monkey C (*t*-test, $P < 0.05$). Deadaptation was incomplete in 5 of 16 sessions (31%) in monkey K and 5 of 13 sessions (38%) in monkey C (*t*-test, $P < 0.05$). Incomplete adaptation and deadaptation preclude a full behavioral dissociation between the task kinematics and dynamics. This in turn limits our interpretation of neuronal activity related to these aspects of the reaching movements. However, as subsequently described, the emphasis of our analysis is on the general time course of force-field–related neuronal activity rather than attempting to make a specific claim as to whether the neurons code for movement kinematics or dynamics.

Force-field–related changes in performance were generally not uniform across the eight reaching directions. For example, in monkey K, trajectory perturbations in early force-field trials due to clockwise forces were much more pronounced in the 113 and 293° target directions than in the 23 and 203° directions, thus forming a bimodal distribution of deviation area across target direction (Fig. 3*A*, *top left*, hand paths). This performance distribution was consistent across all clockwise sessions for monkey K (Fig. 3*A*, *top left*; polar plot indicates the across-session deviation area mean ± CIM in each direction). The bimodal tuning was significant (Rayleigh test, $P < 0.001$, indicated by a thick black line along the major axis of the distribution). The trajectory perturbations due to counterclockwise forces were distributed bimodally as well, although the distribution was oriented differently (Fig. 3*A*, *bottom left*). Therefore the directional dependence of trajectory errors was force-field specific. This directional tuning and force-field specificity could also be seen in the early washout trials, where trajectory perturbations were due to adaptation aftereffects

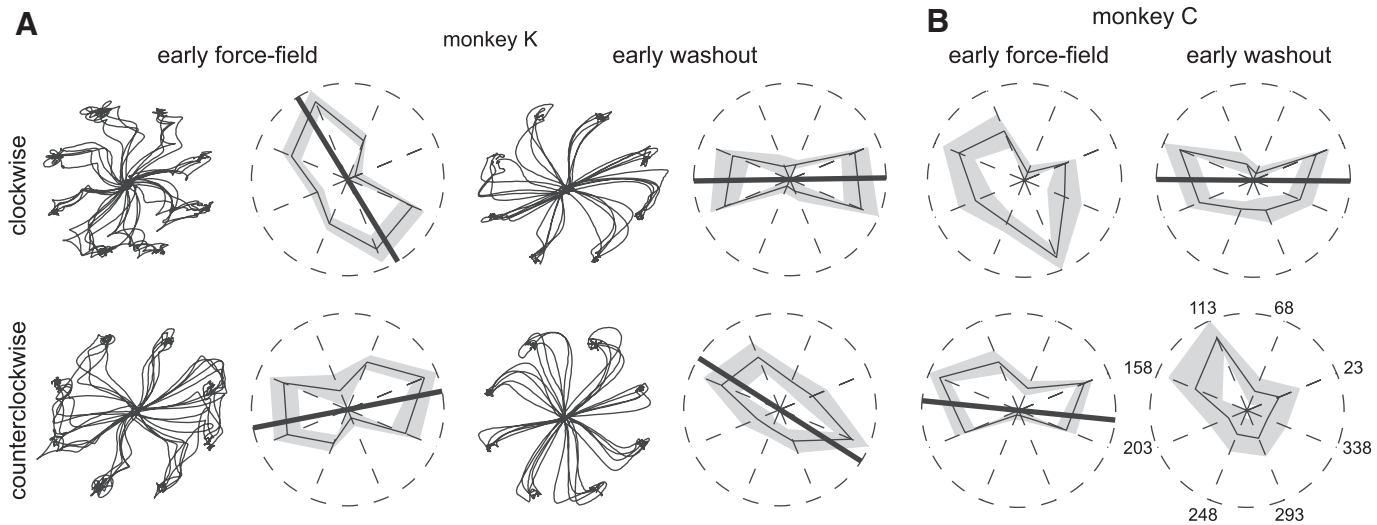

FIG. 3. Anisotropy of behavioral performance. *A*: polar plots show the baseline-corrected average performance in each target direction during the first 40 force-field epoch trials (*left column*) or first 40 washout epoch trials (*right column*) across all clockwise (*top row*) or counterclockwise (*bottom row*) sessions for monkey K. Performance is quantified by the deviation area and the gray regions indicate the 95% CIM. The scale for the radial axis differs slightly for each plot and was excluded since only the relative performance magnitude across directions is pertinent. Thick black lines indicate the major axis when there was significant bimodal directional tuning (Rayleigh test, $P < 0.025$). Next to each polar plot are example hand paths from one session, in which the performance anisotropy can be seen directly. *B*: polar plots as in *A* for monkey C.

instead of applied forces (Fig. 3*A*, *right*). There was a correspondence in directional tuning between clockwise-deviated trajectories and counterclockwise-deviated trajectories regardless of the source of the deviation: direct perturbation from applied forces or aftereffects of learned forces. These observations were generally seen in monkey C as well (Fig. 3*B*), although the clockwise-deviated trajectories did not have significant unimodal or bimodal directional tuning (Rayleigh tests, $P > 0.01$). Nevertheless, the specific clockwise and counterclockwise performance distributions across targets generally corresponded between the two monkeys. Finally, nearly the same directional tuning was seen in adaptation and deadaptation changes (data not shown). Thus adaptation and deadaptation were most evident in movements that incurred the largest initial deviations.

Since the perturbing forces were proportional to hand speed, we next analyzed whether hand speed varied across reaching directions. We found that peak speed was indeed significantly modulated by movement direction, with tuning curves nearly identical to those shown in Fig. 3. Thus the directional tuning of trajectory deviations in the velocity-dependent force fields could be explained by the directional tuning of movement speeds. Anisotropies in the mechanical impedance of the limb coupled to the force-producing manipulandum may explain the directional dependence of movement speed.

Finally, both monkeys also participated in some control sessions, in which a full 480 trials were performed but no novel forces were applied ($n = 4$ sessions, monkey K; $n = 9$ sessions, monkey C). In these control sessions, the frequency of significant adaptation, aftereffect, or deadaptation was less than expected by chance (i.e., <5% of the tests). Therefore the significant behavioral effects seen during sessions with force fields were clearly related to the forces and not to nonspecific effects such as fatigue.

Neuronal database

During each of the behavioral sessions, we recorded extracellularly from neurons in the cingulate motor areas (CMA) of the left hemisphere (Fig. 4*A*, region inside dashed lines). The dorsoventrally oriented electrode penetrations were made several millimeters lateral of the midline so that they first reached the superior frontal gyrus, then passed through white matter to reach the dorsal bank of the cingulate sulcus, and finally through the sulcus to the ventral bank of the cingulate sulcus (Fig. 4*B*). This approach provided a clear anatomical delinea-

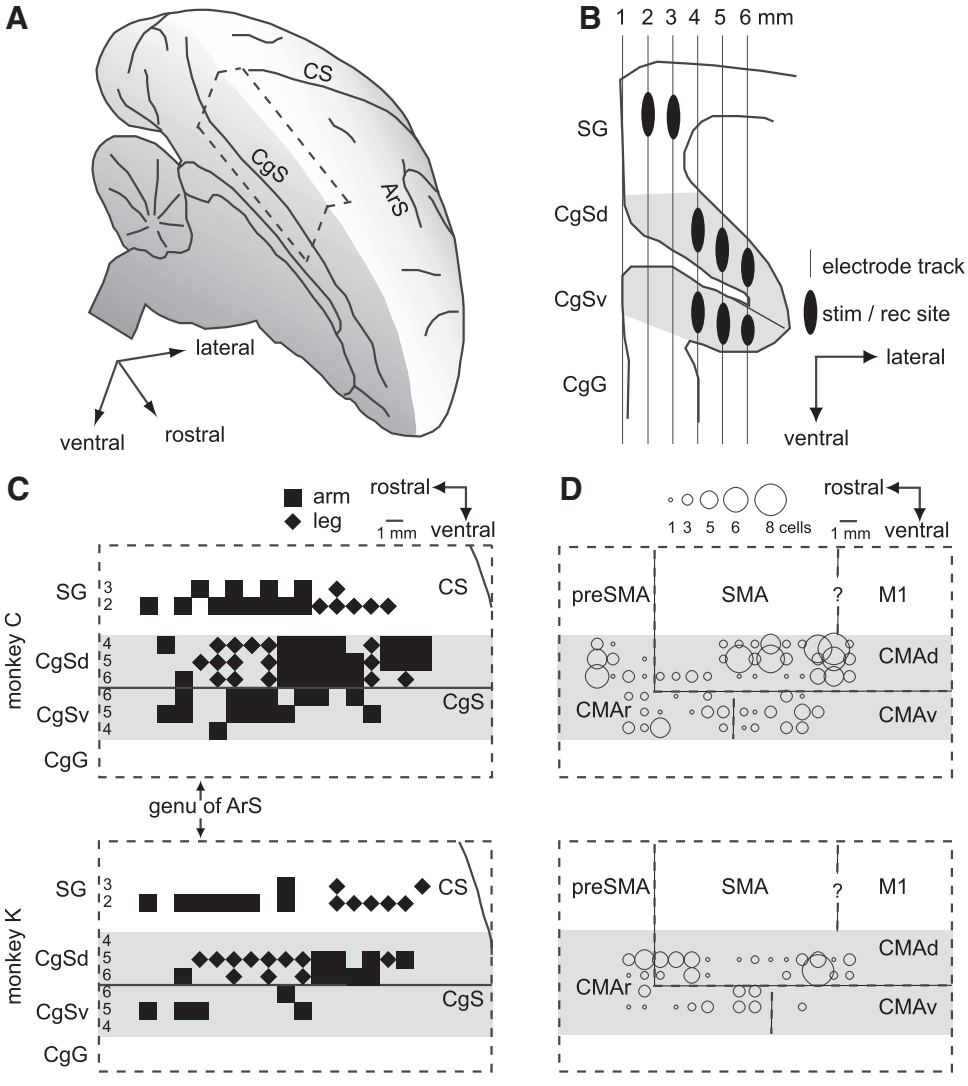

FIG. 4. Neural recording locations. *A*: schematic of the left hemisphere of a rhesus macaque brain. The dashed lines indicate the recording area shown in *B* (coronal view) and *C* and *D* (flattened sagittal view). CS, central sulcus; ArS, arcuate sulcus; CgS, cingulate sulcus. *B*: approximate mediolateral extent of stimulating and recording sites (black ovals). Elongated ovals used to indicate that the exact depth or cortical layer of each site was not known (see METHODS). SG, superior frontal gyrus; CgSd and CgSv, dorsal and ventral banks of cingulate sulcus, respectively; CgG, cingulate gyrus. *C*: intracortical microstimulation (ICMS) results for each monkey. Numbers on the *left* indicate the lateral coordinate in this "flattened" sagittal view. *D*: number of cells recorded at each cortical location in each monkey (circles). Dashed lines indicate approximate boundaries between cortical motor areas based on ICMS results.

tion of the cingulate, although left some of the cingulate sulcus (e.g., the fundus) unexplored.

Prior to the recording sessions, ICMS was applied to map the cortical limb representations. The results for each monkey are shown in Fig. 4*C*. The ICMS maps were quite consistent between the two monkeys. In the superior frontal gyrus, leg movements were evoked caudally and arm movements were evoked rostrally. The dorsal bank of the cingulate sulcus had three separate arm representations interleaved with two leg representations. Finally, only arm movements were evoked along the rostrocaudal extent of the ventral bank of the cingulate sulcus. These maps are largely congruent with maps from other ICMS and anatomical studies (He et al. 1995; Luppino et al. 1991).

The recording locations are shown in Fig. 4*D*. Based on the ICMS maps and their relationship to a previous anatomical study (He et al. 1995), cells were assigned to one of the three cingulate motor areas as depicted by the dashed lines in Fig. 4*D*. In particular, on the dorsal bank, the dividing line between rostral CMA (CMAr) and dorsal CMA (CMAd), i.e., between cytoarchitectonic areas 24c and 6c, was taken to be the most rostral arm-to-leg representation transition of the dorsal bank. This was near the level of the genu of the arcuate sulcus. On the ventral bank, the dividing line between CMAr and ventral CMA (CMAv), i.e., between areas 24c and 23c, was taken to be at the level of the next most rostral arm-to-leg representation transition of the dorsal bank.

Overall, 221 cells were recorded: 81 in CMAr, 107 in CMAd, and 33 in CMAv. Histological analysis confirmed that all of these cells were in the cingulate sulcus. To place the cingulate activity into context, several of the neuronal analyses were performed on previously recorded cells from other cortical motor areas. These include 198 primary motor cortex (M1) cells (Rokni et al. 2007), 142 dorsal premotor cortex (PMd) cells (Xiao et al. 2006), and 298 supplementary motor cortex (SMA) cells (Padoa-Schioppa et al. 2004).

Neuronal activity

OVERVIEW. The activity of each neuron was characterized by the instantaneous spike rate over three perievent time windows of each trial (center hold/instructed delay time, reaction/movement time, and target hold time; see Fig. 1*B*) and three trial epochs of each session (baseline trials, force-field trials, washout trials). An example of the full time-and-trial evolution of spike rate for one CMAd neuron is shown in Fig. 5*A*. Movement onset (*mo*) was reliably correlated with a phasic increase in spike rate throughout the recording session. In contrast, the cell was very quiet around the visual cue presentation and after movement end (*me*) during the target hold time. During the early force-field epoch, the movement-related activity was noticeably enhanced in both amplitude and duration. The spike rate somewhat attenuated during the force-field epoch and then returned to the baseline level during the washout epoch.

To simplify this analysis for each cell, we looked at activity related to intratrial events (i.e., event-related activity) and activity related to intertrial changes in applied forces (i.e., force-field–related activity) separately. Event-related activity was based on the average activity in the last 120 trials of the baseline epoch (Fig. 5*B*) and is described in the next subsection. Force-field–related activity was based on the average activity in a window around movement onset (Fig. 5*C*) and is described in the last subsection.

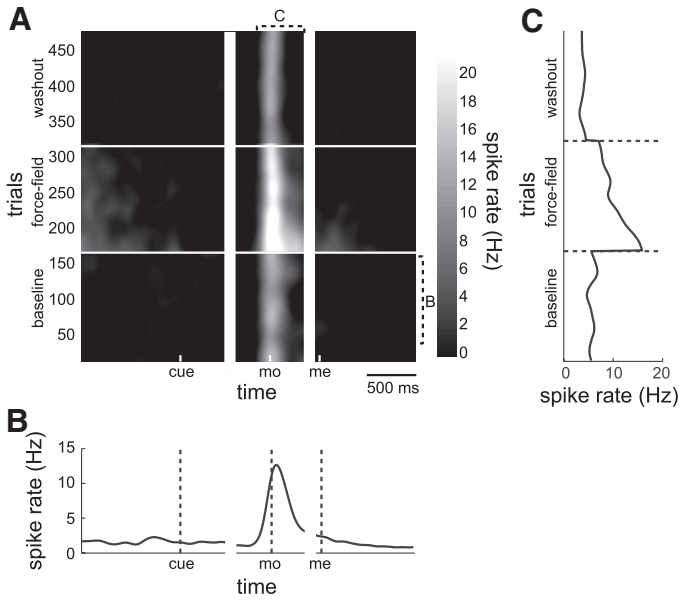

FIG. 5. Example of event-related and force-field–related activity in a dorsal cingulate motor area (CMAd) neuron. *A*: neuronal spike rate shown both within trial [visual cue-aligned, movement onset (mo)-aligned, and movement end (me)-aligned windows] and across trials (baseline, force-field, and washout epochs). Spike rate computed by convolving the aligned spike raster with a 2-dimensional Gaussian window (SDs: 50 ms and 10 trials). *B*: event-related activity during the baseline epoch. *C*: force-field–related activity around movement onset.

EVENT-RELATED. We first investigated how cingulate neurons were engaged in the baseline reaching task, in the absence of applied forces. As an initial step, we evaluated whether there was any modulation of activity by computing a modulation index for each cell. The index ranged from 0 (no modulation) to 1 (continuous modulation) and was based on the average instantaneous spike rate and its confidence interval (see METHODS). However, the spike rate was often a function of the direction of the movement, as the example in Fig. 6*A* demonstrates. A spike raster plot of the last 120 baseline epoch trials, ordered by target direction, clearly indicates that the movement-related activity of this cell was directionally tuned (Fig. 6*A*, *bottom*). When tuning was significant, as determined by a permutation test, the mean instantaneous spike rate was based on the activity in the four directions closest to the preferred direction (i.e., preferred-hemifield average) rather than on the activity in all eight directions (Fig. 6*A*, *top*; see METHODS). The modulation index for the example in Fig. 6*A*, calculated using the preferred-hemifield average, was 0.76. Significant modulation, established using surrogate data, was an index >0.16 (see METHODS).

The modulation index further confirmed the location of the limb representations in the cingulate sulcus. The average modulation index as a function of rostrocaudal location on the dorsal bank of the cingulate sulcus is shown in Fig. 6*B*. As expected, dorsal bank cells in the two ICMS-defined leg representations were much less modulated by the reaching task than cells in the three arm representations. On the ventral bank the average index was always significant, ranging from 0.3 to 0.5.

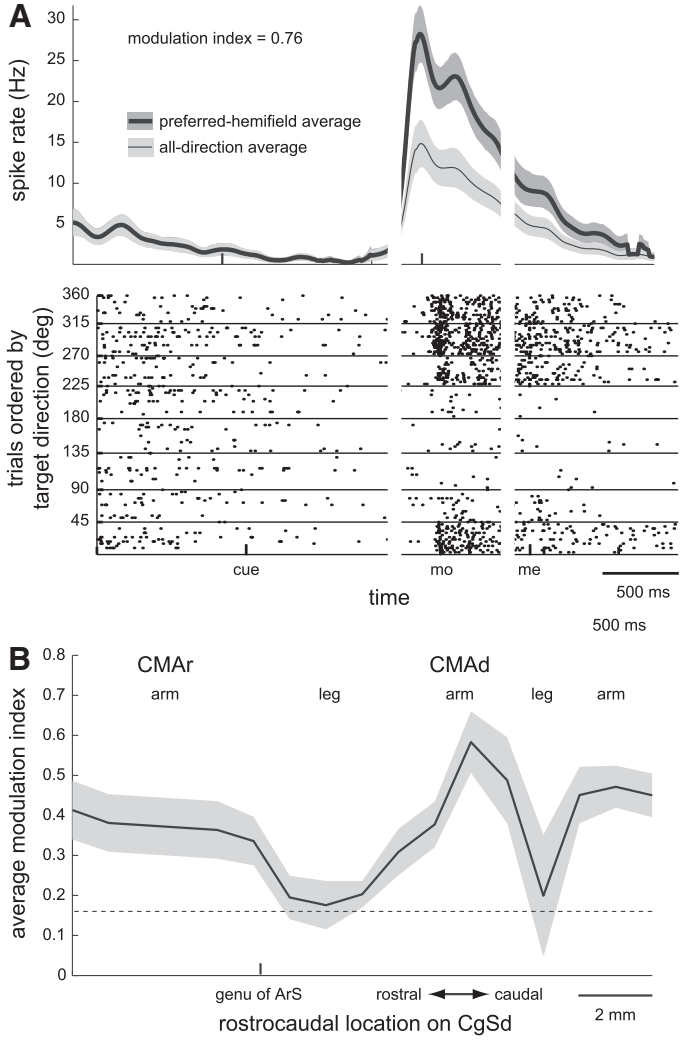

FIG. 6. Influence of target direction and recording location on event-related activity. *A*: example of directionally tuned, baseline-epoch activity in a CMAd neuron. Trials in the spike raster plot (*bottom*) are arranged by target direction to show how movement-related activity is selective for only certain directions. The directional selectivity is captured in the mean instantaneous spike rate (*top*) by averaging only over trials in the 4 directions closest to the preferred spike direction (i.e., by the preferred-hemifield average; gray regions are 95% CIM). *B*: average modulation index (see METHODS) of cells recorded on the dorsal bank of the cingulate sulcus (CgSd) as a function of the rostrocaudal coordinate of the recording site (gray region indicates 95% CIM). Data combined across both monkeys after aligning rostrocaudal coordinates at the level of the genu of the arcuate sulcus (ArS). Significant modulation is an index above the horizontal dashed line. Labels for cortical areas and arm/leg representations are corroborated by the ICMS results (Fig. 4*C*).

Overall, 163 of the 221 recorded cells were significantly modulated (index >0.16) and located within ICMS-defined arm representations: 54 in CMAr, 84 in CMAd, and 25 in CMAv. Only these 163 cells were included in the remainder of the analysis. Furthermore, due to the small sample of CMAv cells and their functional similarity to CMAd cells, we combined CMAv and CMAd cells into a single caudal cingulate (CMAc) data set to compare with CMAr.

After identifying the significantly modulated cells, we next evaluated what types of event-related activity were present in the population. The *k*-mean clustering algorithm was used to define groups of cells with similar event-related activity (see METHODS). Clustering was done on both the normalized instantaneous preferred-hemifield spike rate and the instantaneous directional tuning significance of each cell. The results of the cluster analysis are shown in Fig. 7*A*. For the instantaneous spike rate, five clusters captured the major patterns of event-related activity (Fig. 7*A*, *top left*). Excitatory movement-related activity, both tonic (cluster 1) and phasic (cluster 3), was the most prominent pattern. Smaller numbers of cells had inhibitory (cluster 2) or excitatory (cluster 4) responses during the instructed delay time following the visual cue. Cluster 5 exhibited a ramping up of spike rate during the postmovement, target hold period. There was a trend toward a higher proportion of CMAc cells in the two movement-related activity clusters and a higher proportion of CMAr cells in the pre- and postmovement activity clusters (Fig. 7*A*, *top right*). However, the only cluster in which the proportions were significantly different was cluster 3 [$\chi^2(1) = 8.37$, $P = 0.004$].

For the instantaneous directional tuning significance, three clusters captured the event-related tuning patterns (Fig. 7*A*, *bottom left*). Consistent phasic (cluster 1) or tonic (cluster 3) tuning during movement was seen in a minority of cells. Most cells exhibited little or only intermittent tuning (cluster 2). Very little premovement, preparatory tuning was observed. Clusters 1 and 3 had a significantly higher proportion of CMAc cells [$\chi^2(1) = 4.36$, $P = 0.04$ and $\chi^2(1) = 4.96$, $P = 0.03$, respectively], whereas cluster 2 had a higher proportion of CMAr cells [$\chi^2(1) = 10.84$, $P = 0.001$; Fig. 7*A*, *bottom right*]. Thus directional tuning was more prevalent in the caudal than in the rostral cingulate.

The results of the cluster analysis were somewhat subjective since the number of clusters was not directly inferred from the data. Therefore we performed a second, more conventional analysis of event-related activity. We analyzed the average spike rate in four, 500-ms perievent windows to identify visual cue-related, instructed delay–related, movement-related, and target hold–related activity (see METHODS). The activity in each of these windows was compared with the activity in a control period, the center hold, using a two-way ANOVA (factors: window, target direction). The percentage of significant ($P < 0.05$) main effects of window (Fig. 7*B*, *top*) and window × direction interaction effects (Fig. 7*B*, *bottom*) for CMAr and CMAc are shown. In addition, to provide context to the results, this analysis was repeated for previously obtained data sets from M1, PMd, and SMA.

Significant cue-related activity was more prominent in CMAr than that in CMAc [48 vs. 30%, $\chi^2(1) = 4.4$, $P = 0.03$]. However, the proportion of delay-related (46 vs. 38%), movement-related (78 vs. 86%), and target hold–related (54 vs. 65%) activity did not significantly differ between CMAr and CMAc (Fig. 7*B*, *top*). Relative to noncingulate areas, the amount of cue-related activity in CMAr was nearly the same as that in M1 and SMA (both 47%), but less than that in PMd (62%). The proportion of movement-related activity was similarly large in all five cortical motor areas, ranging from 78 to 90%.

The tuning results for CMAr and CMAc shown at the *bottom* of Fig. 7*B* largely mirror the cluster directional tuning analysis despite the difference in tuning significance criteria. Movement-related and target hold–related tuning were much higher in CMAc than in CMAr [36 vs. 6%, $\chi^2(1) = 16.87$, $P < 0.0001$ and 29 vs. 7%, $\chi^2(1) = 10.11$, $P = 0.002$]. Neither area had

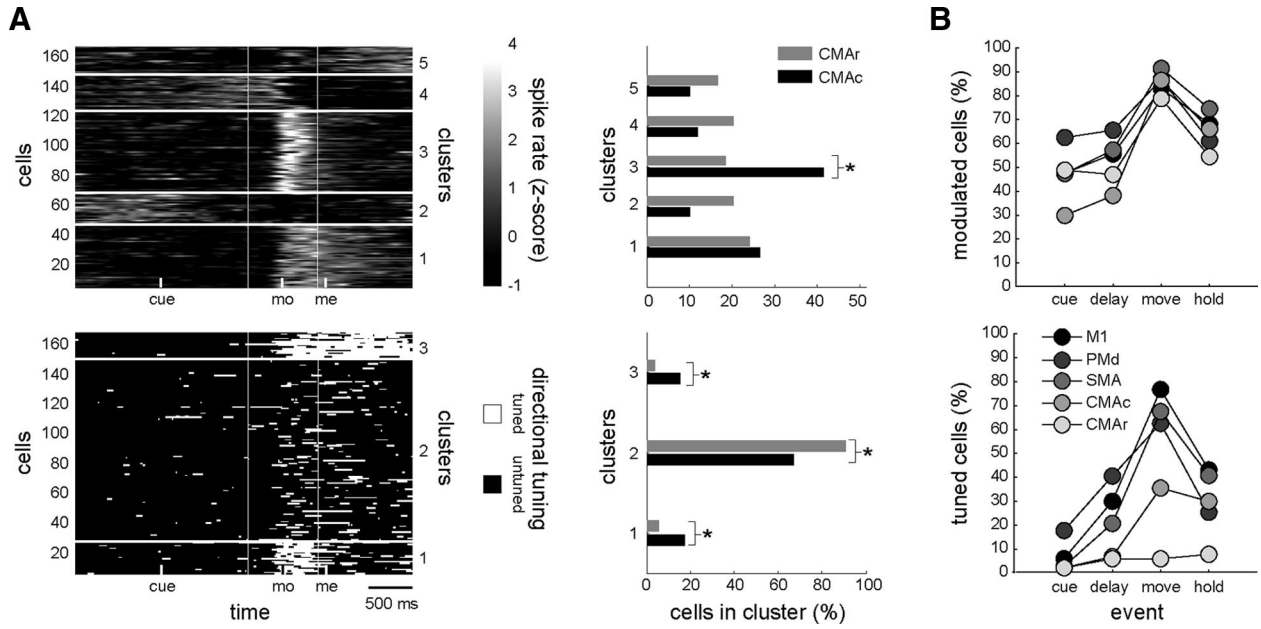

FIG. 7. Summary of event-related activity. *A*: cluster analysis (only CMA cells included). K-means clustering of the instantaneous spike-rate profiles (*top left*) and instantaneous directional tuning significance (*bottom left*). Bar graphs (*right*) indicate the percentage of rostral CMA (CMAr) and caudal CMA (CMAc) cells in each cluster. An asterisk identifies clusters in which the proportion of CMAr and CMAc cells significantly differ (χ^2 test, $P < 0.05$). *B*: ANOVA (cells from 5 cortical motor areas included). Percentage of cells with significant modulation of average spike rate (*top*) or with significant directional tuning (*bottom*) after visual cue presentation, during the instructed delay time, during movement time, and during target hold time (2-way ANOVA, $P < 0.05$).

much directional tuning prior to movement. This is in contrast to M1, PMd, and SMA, all of which had a relatively large amount of tuning during the premovement instructed delay (Fig. 7*B*, *bottom*). Compared with the noncingulate areas, the amount of directional tuning in CMAc was much less during movement (76, 62, 67 vs. 36%), but was comparable during the target hold (42, 25, 40 vs. 29%).

In summary, CMA neurons were engaged in every aspect of the visuomotor reaching task. CMAr cells were more responsive than were CMAc cells to the visual cue instructing the upcoming movement. The majority of cells in both areas were excited around movement onset, with CMAc cells responding more phasically than CMAr cells. Finally, movement-related direction tuning was much more prominent in CMAc than that in CMAr, although the amount of CMAc tuning was modest compared with that of noncingulate cortical motor areas.

FORCE-FIELD–RELATED. Next, we investigated how CMA neurons responded to the applied force fields. An initial inspection found that force-field–related responses almost always occurred during movement, which is the only time the forces were applied since they were velocity dependent. Therefore we looked at the average activity in a window from 100 ms before movement onset to 400 ms after movement onset. Following the analysis used in the previous section, the *k*-mean clustering algorithm was used to define groups of cells with similar across-trial profiles of movement activity. For the across-trial profiles, only the last 40 trials of the baseline epoch and first 40 trials of the washout epoch were used since our interest was primarily in characterizing activity changes occurring around the epoch transitions and within the force-field epoch. Note that for all 163 neurons, the activity during the movement time was significantly modulated across trials, as determined by a modulation index analogous to the one used in the previous section (see METHODS).

Three clusters captured the major patterns of activity modulation (Fig. 8*A*, *top*). In cluster 1 (45% of all CMA cells), the spike rate in the movement window monotonically increased throughout the session. In cluster 2 (26% of all CMA cells), the spike rate suddenly increased at the beginning of the force-field epoch, ramped downward, and then suddenly decreased at the beginning of the washout epoch, as the example in Fig. 5 shows. In cluster 3 (29% of all CMA cells), the spike rate decreased throughout the session, although in some cases increased in the washout epoch. A steadily increasing spike rate across epochs, as in cluster 1, has been observed before and may be related to muscle fatigue or cell injury from the recording electrodes (Li et al. 2001; Padoa-Schioppa et al. 2004). The average patterns in clusters 2 and 3 seem to better reflect a response to the forces, either excitatory (cluster 2) or inhibitory (cluster 3), since they are correlated with the "OFF–ON–OFF" pattern of force application across the three epochs.

Claims of force-field–related activity can be greatly strengthened by looking at the proportion of cells in each cluster that were either recorded during sessions with clockwise or counterclockwise force fields ($n = 99$ cells) or recorded during control sessions in which no novel forces were applied ($n = 64$ cells). These proportions are indicated in the bar graph in Fig. 8*A* (*middle*). Cluster 2 included significantly more cells recorded during sessions with force fields than during control, null-field sessions [$\chi^2(1) = 8.74$, $P = 0.003$]. This was not the case, however, for cluster 3. Therefore the cells in cluster 2 but not cluster 3 may be regarded as having force-field–related activity. Note, however, that the proportion of cells in cluster 2 recorded in null-field sessions was not insignificant (13%), indicating that the cluster analysis did not completely isolate force-field effects from nonspecific effects. Cluster 1 included significantly more cells from null-field sessions than from force-field sessions [$\chi^2(1) = 6.61$, $P = 0.01$], further indicating

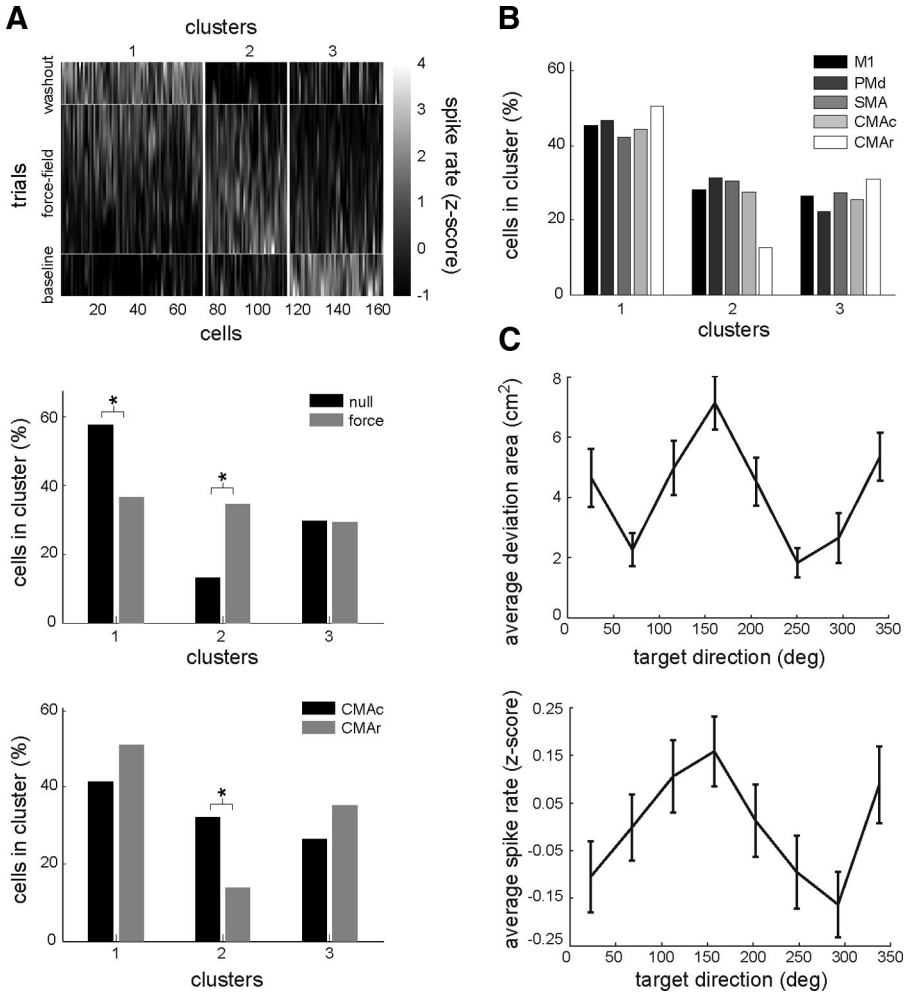

FIG. 8. Summary of force-field–related activity. *A*: cluster analysis (only CMA cells included). K-means clustering (*top*) of across-trial, movement-related spike-rate profiles. Bar graphs indicate the percentage of cells recorded in a null field or a force field in each cluster (*middle*) and the percentage of CMAr and CMAc cells in each cluster (*bottom*). An asterisk identifies clusters in which the proportion of null-field vs. force-field cells or CMAr vs. CMAc cells significantly differ (χ^2 test, $P < 0.05$). *B*: cluster analysis (cells from 5 cortical motor areas included). Across-trial spike-rate profile clusters were qualitatively the same as those shown in *A*. The percentage of cells from each area in each cluster is shown. *C*: anisotropy of behavioral and CMA neuronal response to perturbations. Shown are the baseline-subtracted average performance (*top*; same as in Fig. 3) and average spike rate (*bottom*) in each target direction during the first 40 force-field epoch trials across all clockwise or counterclockwise sessions for both monkeys.

that this pattern of activity is generally not related to the applied forces. We also quantified the number of CMAr and CMAc cells in each cluster (Fig. 8*A*, *bottom*). There were proportionally more CMAc cells in cluster 2 than CMAr cells [$\chi^2(1) = 6.01$, $P = 0.01$]. Thus force-field–related activity was more prominent in the caudal than in the rostral cingulate.

The cluster analysis was repeated after including the M1, PMd, and SMA data sets to determine whether the force-field–related activity seen in cluster 2 was unique to the CMA. The clustered spike-rate profiles (not shown) were qualitatively the same as, and ordered to correspond with, those shown in Fig. 8*A*. Again, cluster 2 included significantly more cells recorded during force-field sessions than control sessions [$\chi^2(1) = 8.41$, $P = 0.004$]. Importantly, the proportion of M1, PMd, SMA, and CMAc cells in cluster 2 did not significantly differ (28, 31, 30, and 28%, respectively; Fig. 8*B*). Therefore the force-field–related activity identified by this analysis was relatively common to all the cortical motor areas except CMAr.

Again due to the somewhat subjective nature of the cluster analysis, we sought further evidence that cingulate neuronal activity was specifically modulated by the applied forces. As noted previously, a specific feature of the behavior in these monkeys was a bimodal distribution of performance across target directions (Fig. 3). This distribution for the deviation area measure in the early force-field epoch, combined across the two monkeys and two types of force fields, is shown again in the *top plot* of Fig. 8*C*. We asked whether the early force-field activity of the cingulate neurons, normalized by subtracting the baseline activity in each direction, had a similar distribution. Indeed the average neuronal response to the forces fields was, like the deviation area, greater around the 158 and 338° target directions (Fig. 8*C*, *bottom*). The two bimodal distributions were significantly correlated (Spearman's rank correlation coefficient, $r = 0.76$, $P = 0.04$). Thus on average, the neuronal response in the early force-field epoch tended to be greatest in movement directions that experienced the largest perturbations.

The preceding analysis of force-field–related activity dealt only with average spike rate during movement. Yet previous work has found that the most specific correlates of force-field adaptation are in the directional tuning changes. In particular, adaptation to velocity-dependent curl force fields like those used in this study has been shown to be correlated with a rotation of the preferred direction (PD) of the tuning curve of both muscle activity (Shadmehr and Moussavi 2000; Thoroughman and Shadmehr 1999) and cortical activity (Li et al. 2001; Padoa-Schioppa et al. 2004; Xiao et al. 2006). To explore this possibility, we first looked at the distribution of PDs across the population. The PD distribution of movement-related activity in the baseline epoch, combining both CMAr and CMAc cells, was significantly bimodal (Rayleigh test, $P < 0.0001$) and oriented along the 150–330° axis (Fig. 9*A*). The PD distributions in the force-field and washout epochs were

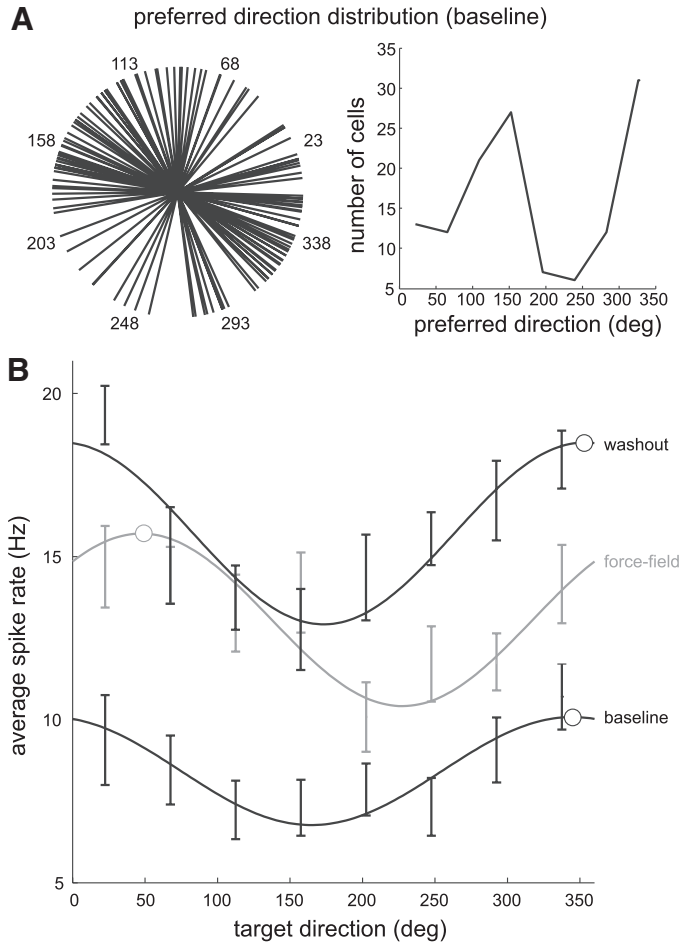

FIG. 9. Force-field–related activity and directional tuning. *A*: distribution of preferred directions for the CMA population, based on baseline epoch activity. *B*: example of change in directional tuning in one CMAc neuron. The force field was counterclockwise. Average spike rate (±CIM) in each target direction and each epoch is shown along with cosine fits. Open circles mark the preferred direction of each tuning curve.

similarly bimodal. Interestingly, this bimodal distribution was very similar to the distributions of the behavioral and neural responses to force-field perturbation shown in Fig. 8*B* (Spearman's rank correlation coefficient, $r = 0.77$, $P = 0.03$ and $r = 0.57$, $P = 0.13$, respectively).

Second we looked for PD shifts between epochs. For this analysis, only cells that had significant movement-time directional tuning in all three epochs were included. There were too few CMAr cells tuned in all three epochs ($n = 8$) to perform the analysis. In CMAc, 52 cells were tuned in all three epochs: 30 cells from clockwise or counterclockwise sessions and 22 cells from control sessions. In the control sessions, as expected, there was no consistent pattern of PD shifts; the baseline to force-field epoch shifts were uncorrelated with the force-field to washout epoch shifts (Rokni et al. 2007). However, in the clockwise and counterclockwise sessions there were several examples of the pattern of PD shifts seen in previous studies. One such example is shown in Fig. 9*B*. In this example CMAc cell, from a counterclockwise force-field session, there was an increase in average spike rate across the three epochs, as seen in many cells (Fig. 8*A*). Importantly, however, the force-field epoch tuning curve shifted counterclockwise (i.e., in the direction of the field) relative to the baseline epoch tuning curve and then shifted back in the washout epoch. However, unlike that found in other cortical motor areas, these types of shifts were not significant at the population level in CMAc. Neither the baseline to force-field epoch population PD shift ($n = 30$, mean = 4.49°; the sign of shifts from clockwise sessions was reversed so that all positive shifts were in the direction of the field) nor the force-field to washout epoch population PD shift ($n = 30$, mean = −4.46°) was significantly different from zero (circular *t*-test, $P > 0.05$).

In summary, average movement-related activity was modulated by applied forces in a minority of cingulate neurons. These changes were more likely to occur in CMAc than in CMAr and roughly scaled with the amount of perturbation in each direction. Finally, directional tuning of movement-related activity was not systematically modulated by the force fields.

DISCUSSION

In the present study, we examined how neurons in the cingulate motor areas were involved in controlling visually instructed reaching movements in both normal and altered environments. We found that the cingulate neuronal activity was modulated during preparation and control of reaching and in response to applied forces. CMAr neurons were modulated by the visual instruction to a greater extent than that in CMAc neurons. However, CMAc neurons had a greater amount of phasic and directionally tuned activity during movement than that in CMAr cells. Furthermore, compared with CMAr cells, the movement-related activity of CMAc cells was more frequently modulated by the applied force fields. Other interesting features of the data were the directional dependence of the behavioral and neuronal responses to perturbations and the nonuniformity of direction representation in the cingulate. The initial errors caused by the force fields were distributed bimodally across target directions. A very similar bimodal distribution was seen in the average neuronal response to the perturbation and in the distribution of preferred directions (PDs).

Limitations

One limitation of our study was in treating CMAc as a single area rather than two separate areas: CMAd and CMAv. Although this has often been done (Crutcher et al. 2004; Shima and Tanji 1998; Shima et al. 1991), there are many anatomical reasons why CMAd and CMAv should be considered two distinct cortical motor areas, as summarized in He et al. (1995). Another limitation is that the behavioral task used in our study did not permit an analysis of reward-related neuronal activity. Previous work has suggested that CMAr cells are involved in processing reward information (Akkal et al. 2002; Hadland et al. 2003; Shidara and Richmond 2002; Shima and Tanji 1998; Williams et al. 2004). A ramping up of activity leading to the reward was observed in some cells (see cluster 5 in Fig. 7*A*, *top left*) and it occurred more often in CMAr than in CMAc. In our task, however, the reward was delivered following a 1-s target hold period and subsequently the monkey was immediately free to make a movement back to the center to begin the next trial. Thus it was not possible to dissociate whether activity occurring around the time of the reward was

related to the reward itself or to preparation or execution of the return movement back to the center. Furthermore, the percentage of unrewarded, aborted trials in each session due to behavioral errors was quite low (6.2 ± 3.5%, mean ± SD), making a statistical analysis of activity in such trials impractical.

Comparison of CMAr and CMAc

CMAr has previously been found to lack much of a directionally selective response either to visual stimuli or during movement (Akkal et al. 2002; Hoshi et al. 2005). This is surprising in that all other known cortical motor areas, including CMAc (Crutcher et al. 2004; Russo et al. 2002), show ample amounts of directional tuning. As a result, it has been suggested that CMAr functions at a relatively "high level" (Akkal et al. 2002).

Previous work has also identified a rostrocaudal gradient in sensorimotor function of cingulate neurons. Similar to our observations, these studies found that CMAr cells were proportionally more active during an instruction stimulus and movement preparation, whereas CMAc cells were proportionally more active during movement execution (Shima and Tanji 1998; Shima et al. 1991). A rostrocaudal gradient has also been observed within CMAr: the most rostral parts of CMAr responded more to visual instruction and the more caudal parts responded to movement preparation (Hoshi et al. 2005). This rostrocaudal functional gradient is similar to that seen between premotor and primary motor areas on the lateral surface of the hemisphere (Kalaska and Crammond 1992). Further evidence that CMAc is more involved than CMAr in movement execution is that movement-related CMAc activity was more often modulated by forces, as discussed in the following text.

Force-field–related activity in the cingulate

Movement-related activity in the cingulate was modulated by applied loads: 32% of CMAc cells and 14% of CMAr cells had a rapid increase in spike rate on application of forces, followed by a gradual decrease in activity over the course of adaptation, and finally an abrupt spike rate decrease when the forces were turned off (Fig. 8*A*). Given the relative absence of this pattern in the control sessions, it is clear that the activity of these cells reflects some aspect of the perturbation or compensatory response. However, whether the activity reflects the kinematic error or kinetic response is not immediately apparent. As we noted previously, behavioral adaptation was incomplete in about 45% of sessions and thus the kinematic and kinetic aspects of the task were often never complete dissociated.

Studies using human subjects have found that adaptation to force fields is generally achieved by two complementary mechanisms: by modulating limb impedance through cocontraction of antagonistic muscles and by generating feedforward commands from a predictive model of the perturbation (Franklin et al. 2003; Thoroughman and Shadmehr 1999). The former is used initially, when the forces are novel, and the latter is used after repeated practice, once an internal model has been learned. Thus in principle, the profile of force-field–related activity follows the time course of the cocontraction mechanism. So we may tentatively interpret the force-field–related activity in the cingulate as a correlate of the greater muscular effort needed in the early force-field epoch, which slowly decreases as the motor system learns to adjust the feedforward commands. However, the conclusion that the CMAc is important to a cocontraction or feedback-driven response to the perturbation requires two qualifications. First, the applied force response was just as prominent in M1, PMd, and SMA (Fig. 8*B*), indicating that the CMAc was certainly not unique in this regard. Second, the percentage of cells with force-field–related responses in each of these areas was rather modest, particularly considering that around 10–15% of what was classified as force-field effects may be nonspecific effects (Fig. 8*A*, *middle*).

Next, we can consider whether the CMA was additionally involved in adjusting the feedforward motor commands. For velocity-dependent curl force fields, as used in the present study, the appropriate predictive response is to effectively shift the directional tuning curves of agonist muscles in the direction of the field (Thoroughman and Shadmehr 1999). In other words, the muscle's PD is rotated either clockwise or counterclockwise, depending on the field. Our previous work has found that neurons in primary, supplementary, and premotor cortices (M1, SMA, and PM) also rotate their PDs in the direction of the applied field during the force-field epoch and then rotate back in the washout epoch (Li et al. 2001; Padoa-Schioppa et al. 2002, 2004; Xiao et al. 2006). Although this pattern of PD shifts was observed in several cells (e.g., Fig. 9*B*), the shifts were not significant across the population of CMA cells. Therefore the cingulate may play less of a role in generating feedforward compensatory commands relative to other cortical motor areas.

Bimodal directional selectivity

Although the neuronal PDs did not rotate, they did bear another interesting relationship to the applied loads. The PDs had a bimodal distribution that was very similar to the across-direction variation of behavioral and neuronal responses to force-field perturbations. Nonuniform PD distributions have been reported previously in M1 (Georgopoulos et al. 1982; Kurtzer et al. 2006; Mitsuda and Onorati 2002; Naselaris et al. 2006; Scott and Kalaska 1997; Scott et al. 2001). However, many other reports of PD distributions, including the only such report on CMAc (Russo et al. 2002), concluded that the distributions were uniform. There are at least two reasons for this discrepancy. First, nonuniform PD distributions are correlated with anisotropic mechanical properties of the limb (Scott et al. 2001). Task differences in limb configuration change the degree of mechanical anisotropy and, correspondingly, the distribution of PDs (Scott and Kalaska 1997). Second, the nonuniformity found by us and many others is bimodal, not unimodal, just as the mechanical properties (e.g., endpoint inertia) are bimodal (Hogan 1985). However the standard Rayleigh test, used by Russo et al. (2002) and others, has null and alternative hypotheses of uniformity and unimodality, respectively (Fisher 1993). Bimodal distributions will generally fail to show significance in this test.

The observed bimodal variation of behavioral responses across reaching directions is logical if we assume that the PD distribution is indeed correlated with the mechanical impedance of the limb (Scott et al. 2001). In particular, considering the velocity-dependent perturbing forces were always orthog-

onal to movement direction, the largest deviations in hand path should be seen when reaching orthogonal to the axis of minimum impedance. Thus the largest deviations should occur when moving to targets along the axis of maximum impedance (i.e., ~145–325° axis), which was what we observed.

Finally, the observed bimodal variation of neuronal responses across reaching directions may simply reflect the bimodal variation in behavioral errors through a feedback process. CMAc receives considerable proprioceptive input and has been shown previously to exhibit short-latency, excitatory responses to force perturbations to the hand (Cadoret and Smith 1995, 1997). The percentage of cells with reflex-like responses to perturbations (38%) in Cadoret and Smith (1997) was similar to what we observed (32%). Interestingly, Cadoret and Smith (1997) failed to observe anticipatory responses in the CMAc to predictable force perturbations despite clear behavioral anticipation. This is compatible with our finding that the feedforward component of curl force-field compensation, a shift in directional tuning, was nearly absent in the CMAc. Together, these findings support the conclusion that CMAc is involved more in generating reactive rather than proactive motor commands during adaptation to novel forces.

ACKNOWLEDGMENTS

We thank M. Cantor for technical assistance.

GRANTS

This research was supported by National Institute of Neurological Disorders and Stroke Grant NS-044393.

REFERENCES

Akkal D, Bioulac B, Audin J, Burbaud P. Comparison of neuronal activity in the rostral supplementary and cingulate motor areas during a task with cognitive and motor demands. *Eur J Neurosci* 15: 887–904, 2002.

Backus DA, Ye S, Russo GS, Crutcher MD. Neural activity correlated with the preparation and execution of visually guided arm movements in the cingulate motor area of the monkey. *Exp Brain Res* 140: 182–189, 2001.

Cadoret G, Smith AM. Input–output properties of hand-related cells in the ventral cingulate cortex in the monkey. *J Neurophysiol* 73: 2584–2590, 1995.

Cadoret G, Smith AM. Comparison of the neuronal activity in the SMA and the ventral cingulate cortex during prehension in the monkey. *J Neurophysiol* 77: 153–166, 1997.

Crutcher MD, Russo GS, Ye S, Backus DA. Target-, limb-, and context-dependent neural activity in the cingulate and supplementary motor areas of the monkey. *Exp Brain Res* 158: 278–288, 2004.

Deiber MP, Wise SP, Honda M, Catalan MJ, Grafman J, Hallett M. Frontal and parietal networks for conditional motor learning: a positron emission tomography study. *J Neurophysiol* 78: 977–991, 1997.

Della-Maggiore V, McIntosh AR. Time course of changes in brain activity and functional connectivity associated with long-term adaptation to a rotational transformation. *J Neurophysiol* 93: 2254–2262, 2005.

Dettmers C, Fink GR, Lemon RN, Stephan KM, Passingham RE, Silbersweig D, Holmes A, Ridding MC, Brooks DJ, Frackowiak RS. Relation between cerebral activity and force in the motor areas of the human brain. *J Neurophysiol* 74: 802–815, 1995.

Doyon J, Owen AM, Petrides M, Sziklas V, Evans AC. Functional anatomy of visuomotor skill learning in human subjects examined with positron emission tomography. *Eur J Neurosci* 8: 637–648, 1996.

Dum RP, Strick PL. Motor areas in the frontal lobe of the primate. *Physiol Behav* 77: 677–682, 2002.

Ehrsson HH, Fagergren A, Ehrsson GO, Forssberg H. Holding an object: neural activity associated with fingertip force adjustments to external perturbations. *J Neurophysiol* 97: 1342–1352, 2007.

Fink GR, Frackowiak RS, Pietrzyk U, Passingham RE. Multiple nonprimary motor areas in the human cortex. *J Neurophysiol* 77: 2164–2174, 1997.

Fisher NI. *Statistical Analysis of Circular Data.* New York: Cambridge Univ. Press, 1993.

Franklin DW, Osu R, Burdet E, Kawato M, Milner TE. Adaptation to stable and unstable dynamics achieved by combined impedance control and inverse dynamics model. *J Neurophysiol* 90: 3270–3282, 2003.

Gandolfo F, Li C, Benda BJ, Padoa-Schioppa C, Bizzi E. Cortical correlates of learning in monkeys adapting to a new dynamical environment. *Proc Natl Acad Sci USA* 97: 2259–2263, 2000.

Georgopoulos AP, Kalaska JF, Caminiti R, Massey JT. On the relations between the direction of two-dimensional arm movements and cell discharge in primate motor cortex. *J Neurosci* 2: 1527–1537, 1982.

Grafton ST, Hazeltine E, Ivry RB. Abstract and effector-specific representations of motor sequences identified with PET. *J Neurosci* 18: 9420–9428, 1998.

Hadland KA, Rushworth MF, Gaffan D, Passingham RE. The anterior cingulate and reward-guided selection of actions. *J Neurophysiol* 89: 1161–1164, 2003.

He SQ, Dum RP, Strick PL. Topographic organization of corticospinal projections from the frontal lobe: motor areas on the medial surface of the hemisphere. *J Neurosci* 15: 3284–3306, 1995.

Hogan N. The mechanics of multi-joint posture and movement control. *Biol Cybern* 52: 315–331, 1985.

Hoshi E, Sawamura H, Tanji J. Neurons in the rostral cingulate motor area monitor multiple phases of visuomotor behavior with modest parametric selectivity. *J Neurophysiol* 94: 640–656, 2005.

Kalaska JF, Crammond DJ. Cerebral cortical mechanisms of reaching movements. *Science* 255: 1517–1523, 1992.

Kuhtz-Buschbeck JP, Ehrsson HH, Forssberg H. Human brain activity in the control of fine static precision grip forces: an fMRI study. *Eur J Neurosci* 14: 382–390, 2001.

Kurtzer I, Herter TM, Scott SH. Nonuniform distribution of reach-related and torque-related activity in upper arm muscles and neurons of primary motor cortex. *J Neurophysiol* 96: 3220–3230, 2006.

Li CS, Padoa-Schioppa C, Bizzi E. Neuronal correlates of motor performance and motor learning in the primary motor cortex of monkeys adapting to an external force field. *Neuron* 30: 593–607, 2001.

Luppino G, Matelli M, Camarda RM, Gallese V, Rizzolatti G. Multiple representations of body movements in mesial area 6 and the adjacent cingulate cortex: an intracortical microstimulation study in the macaque monkey. *J Comp Neurol* 311: 463–482, 1991.

Mitsuda T, Onorati P. Three-dimensional tuning profile of motor cortical activity during arm movements. *Neuroreport* 13: 1477–1480, 2002.

Moore BR. A modification of the Rayleigh test for vector data. *Biometrika* 67: 175–180, 1980.

Naselaris T, Merchant H, Amirikian B, Georgopoulos AP. Large-scale organization of preferred directions in the motor cortex. I. Motor cortical hyperacuity for forward reaching. *J Neurophysiol* 96: 3231–3236, 2006.

Osu R, Burdet E, Franklin DW, Milner TE, Kawato M. Different mechanisms involved in adaptation to stable and unstable dynamics. *J Neurophysiol* 90: 3255–3269, 2003.

Osu R, Franklin DW, Kato H, Gomi H, Domen K, Yoshioka T, Kawato M. Short- and long-term changes in joint co-contraction associated with motor learning as revealed from surface EMG. *J Neurophysiol* 88: 991–1004, 2002.

Padoa-Schioppa C, Li CS, Bizzi E. Neuronal correlates of kinematics-to-dynamics transformation in the supplementary motor area. *Neuron* 36: 751–765, 2002.

Padoa-Schioppa C, Li CS, Bizzi E. Neuronal activity in the supplementary motor area of monkeys adapting to a new dynamic environment. *J Neurophysiol* 91: 449–473, 2004.

Picard N, Strick PL. Motor areas of the medial wall: a review of their location and functional activation. *Cereb Cortex* 6: 342–353, 1996.

Rokni U, Richardson AG, Bizzi E, Seung HS. Motor learning with unstable neural representations. *Neuron* 54: 653–666, 2007.

Russo GS, Backus DA, Ye S, Crutcher MD. Neural activity in monkey dorsal and ventral cingulate motor areas: comparison with the supplementary motor area. *J Neurophysiol* 88: 2612–2629, 2002.

Scott SH, Gribble PL, Graham KM, Cabel DW. Dissociation between hand motion and population vectors from neural activity in motor cortex. *Nature* 413: 161–165, 2001.

Scott SH, Kalaska JF. Reaching movements with similar hand paths but different arm orientations. I. Activity of individual cells in motor cortex. *J Neurophysiol* 77: 826–852, 1997.

Shadmehr R, Moussavi ZM. Spatial generalization from learning dynamics of reaching movements. *J Neurosci* 20: 7807–7815, 2000.

Shadmehr R, Mussa-Ivaldi FA. Adaptive representation of dynamics during learning of a motor task. *J Neurosci* 14: 3208–3224, 1994.

Shidara M, Richmond BJ. Anterior cingulate: single neuronal signals related to degree of reward expectancy. *Science* 296: 1709–1711, 2002.

Shima K, Aya K, Mushiake H, Inase M, Aizawa H, Tanji J. Two movement-related foci in the primate cingulate cortex observed in signal-triggered and self-paced forelimb movements. *J Neurophysiol* 65: 188–202, 1991.

Shima K, Tanji J. Role for cingulate motor area cells in voluntary movement selection based on reward. *Science* 282: 1335–1338, 1998.

Thoroughman KA, Shadmehr R. Electromyographic correlates of learning an internal model of reaching movements. *J Neurosci* 19: 8573–8588, 1999.

Thoroughman KA, Shadmehr R. Learning of action through adaptive combination of motor primitives. *Nature* 407: 742–747, 2000.

Williams ZM, Bush G, Rauch SL, Cosgrove GR, Eskandar EN. Human anterior cingulate neurons and the integration of monetary reward with motor responses. *Nat Neurosci* 7: 1370–1375, 2004.

Xiao J, Padoa-Schioppa C, Bizzi E. Neuronal correlates of movement dynamics in the dorsal and ventral premotor area in the monkey. *Exp Brain Res* 168: 106–119, 2006.